crystals

MDPI

Article

# Tunable and Polarization-Independent Plasmon-Induced Transparency in a Fourfold Symmetric Metal-Graphene Terahertz Metamaterial

**Guanqi Wang [1], Xianbin Zhang [1,*], Xuyan Wei [1] and Gaoqi Zhang [2]**

[1] Department of Applied Physics, Xi'an University of Technology, Xi'an 710048, China; gqwang@stu.xaut.edu.cn (G.W.); weixuyan113@stu.xaut.edu.cn (X.W.)
[2] School of Automation, Central South University, Changsha 410083, China; wuli2@xaut.edu.cn
* Correspondence: zhangxianbin@xaut.edu.cn; Tel.: +86-29-82066351

Received: 2 November 2019; Accepted: 25 November 2019; Published: 28 November 2019


**Abstract:** The introduction of graphene into metamaterials allows for more flexible and convenient control of electromagnetic waves. In this paper, one simple plasmon-induced transparency (PIT) structure with tunability and polarization independence is investigated in the terahertz (THz) regime. The simulation results indicate that the transparent window can be manipulated in a wide range and even switched off by merely changing the Fermi energy of graphene. By continuously altering the resonance intensity of the dark resonator using the graphene, the PIT resonance can be actively manipulated. The behavior can be elucidated by the classical coupled two-particle model, which corresponds well to the simulation results. Owing to the fourfold symmetric structure, the proposed PIT device exhibits polarization-independent characteristics. This work provides design guidance for metal-graphene THz modulators.

**Keywords:** graphene; metamaterial; plasmon-induced transparency; polarization-independent

## 1. Introduction

The terahertz (THz) wave is in the special region of transition, from macroelectronics to microphotonics, on the electromagnetic spectrum, so it has abundant scientific connotations and unique advantages, which means it has wide application prospects, such as terahertz radar, wireless communication, and bioimaging [1–3]. However, compared with the development of terahertz emission sources and detectors, there is a lack of functional devices for controlling terahertz waves. Therefore, there is an urgent need to develop all kinds of high-performance terahertz functional devices with a high degree of freedom and high efficiency, to promote the development of terahertz technology. Metamaterials, a variety of artificial electromagnetic materials with exotic characteristics relative to natural materials, provide a unique and efficient way to solve this problem. People pay tremendous attention to metamaterials, because they can freely control electromagnetic wave propagation and customize functional devices according to practical needs [4–6]. Among the various metamaterials, the plasmon-induced transparency (PIT) metamaterials have been widely investigated as an important strategy for modulating terahertz waves [7–16]. The PIT effect is a plasmonic analogue of the quantum electromagnetically induced transparency (EIT) effect, which originates from the destructive interference between bright and dark modes in a plasma system and can be flexibly designed and implemented at room temperature.

Metal-based traditional PIT metamaterials can be modulated by carefully changing the geometric parameters of their structure or by modifying substrates, and these ways are too complex to meet the requirements of practical operation in modern compact and convenient THz devices. Therefore, it is

essential to propose the active tunable PIT device for simple operation. Fortunately, in the THz regime, graphene, as a kind of semimetal material with zero band gap, is the best choice for designing and engineering dynamic, tunable PIT devices due to its excellent photoelectric properties [17–19] such as supporting surface plasmas [20–22], lower intrinsic losses [23], and tunable surface conductivity [24–26]. Interestingly, the optical properties of graphene can be modified by applying many stimuluses such as chemical doping, electrostatic gating, and optical pumping [27,28]. Generally, most of the tunable PIT metamaterials are polarization-dependent on the incident terahertz wave (i.e., the response to a fixed polarization), which strongly restrains their practical application in some areas. To address this issue, the use of polarization-independent PIT metamaterials is proposed to achieve a uniform response to arbitrary incident polarization [29–31]. However, the behavior of PIT metamaterials with optical tunability and polarization independence, which can be achieved at a specific resonance frequency without affecting the adjacent frequency spectra, has not been fully investigated.

In the present work, in order to obtain a tunable polarization-independent PIT effect in the THz regime, one simple structure based on metal–graphene is proposed. By integrating graphene into the metal architecture, the tunable property is realized. Here, one metallic closed square ring resonator (CRR) and four identical split ring resonators (SRRs) form a symmetric structure. The numerical simulation results show that the PIT peak can be fully manipulated at a specific resonance frequency by varying the Fermi energy of graphene. Based on the classical coupled two-particle model, it is found that the Fermi energy of graphene plays a decisive role in the manipulation of the transparent window. In addition, the electric field distributions further reveal that the active tunability of PIT metamaterial lies in the manipulation of the dark mode resonance intensity by the conductive graphene layer, allowing for an adjustable current in the dark resonator. Most importantly, based on the symmetrical structure, the proposed PIT device is polarization-independent for incident waves, which provides an obvious advantage for engineering applications. This work provides a new degree of freedom to manipulate PIT metamaterials with graphene and opens up avenues for engineering terahertz wave modulation devices.

## 2. Proposed Structure and Methods

The polarization-independent PIT structure consists of a metallic closed square ring resonator surrounded by four identical split ring resonators, each made of 200-nm-thick aluminum (Al). The details of the geometrical sizes of the meta-atoms are described in Figure 1, and one can clearly see that the structure has a fourfold symmetry (i.e., the structure rotates $2\pi/4$ radians around its geometric center in the x-y plane, and the resulting image coincides with the original image). It is worth noting that to investigate the active modulation in the PIT metamaterial, the graphene layer is covered on the silicon (Si) substrate with relative permittivity $\varepsilon_{si} = 11.7$. In the interesting THz regime, the lossy Al, characterizing the optical properties, can be described by the Drude model as follows:

$$\varepsilon_{Al}(\omega) = \varepsilon_{\infty} - \frac{\omega_p^2}{\omega^2 + i\omega\gamma} \tag{1}$$

where $\omega_p = 11.9 \times 10^4 \text{cm}^{-1}$ and $\gamma = 6.6 \times 10^2$ cm$^{-1}$ are the plasma frequency and the damping constant [32], respectively.

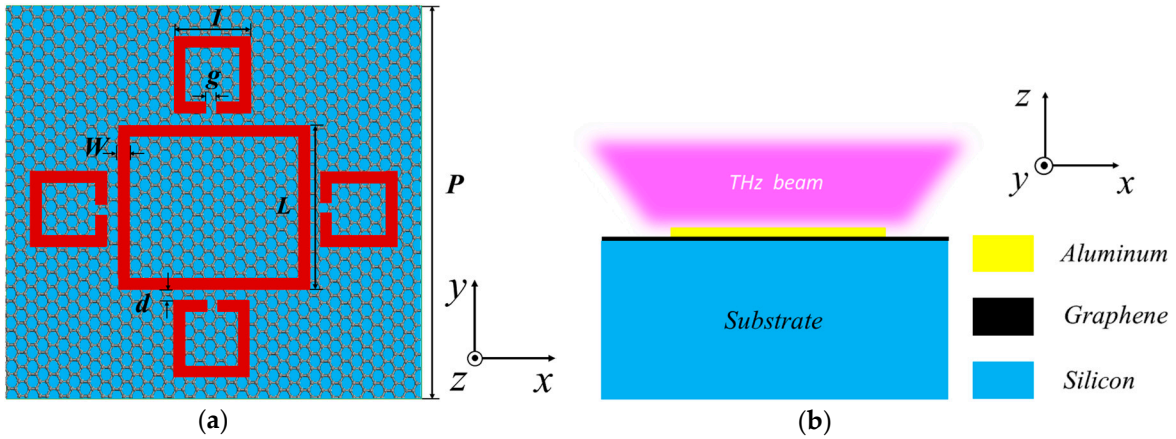


**Figure 1.** (**a**) Top view (from z component) for the unit cell of the polarization-independent plasmon-induced transparency (PIT) metal–graphene metamaterial. The geometrical parameters are: P = 150 μm, L = 71 μm, I = 30 μm, W = 5 μm, g = 5 μm, and d = 5 μm. (**b**) Cross section of the unit cell for the proposed structure.

The main reason why graphene is closely related to terahertz technology, is the unique optical properties it possesses due to its intraband transition and plasma oscillation. Under incident light radiation, the light absorption of graphene involves two processes: intraband transition and interband transition, which can be described by surface conductivity. As the lower frequency of terahertz wave, the interband transition is forbidden, and the intraband transition dominates. In the THz region, by using random-phase approximation (RPA), the surface conductivity of graphene, which closely relates to the Fermi energy, can be derived by the Drude-like model [33] as follows:

$$\sigma_{gra} = \frac{e^2 E_F}{\pi\hbar^2} \frac{i}{\omega + i/\tau}. \tag{2}$$

where $e$ is the electron charge, $E_F$ is the Fermi energy referenced to the Dirac point in graphene, $\omega$ is the incident light radian frequency, $\hbar$ is the reduced Planck's constant, and $\tau = uE_F/\left(ev_F^2\right)$ is the carrier relaxation time. As can be seen from equation (2), the graphene conductivity characteristics can be manipulated by adjusting the Fermi energy $E_F$ via chemical or electrostatic gating. Based on the expression $E_F \propto \sqrt{V_g}$, the external gate voltage $V_g$ can smartly control the Fermi energy $E_F$ [31]. The excellent photoelectric modulation performance of graphene can be used to manipulate THz wave flexibly. In our work, the Fermi velocity is assumed to be$v_F = 1.1 \times 10^6$ m/s and the carrier mobility is chosen as $u = 3000$ cm$^2/(V \cdot s)$, as referenced from experimental measurements [34,35].

To demonstrate the tunable polarization-independent PIT effect, numerical calculations using the finite-difference time-domain (FDTD) method were performed. The FDTD method is one of the important methods for the numerical calculation of electromagnetic fields and requires less memory for computing. For the unit cell, the periodic boundary conditions were employed in both the x and y directions, and the perfectly matched layer (PML) boundary condition was utilized for the z direction to maintain computational convergence. The linearly polarized terahertz wave propagated along the negative $z$-axis, and a frequency-domain power monitor was placed at the bottom of the substrate to detect the transmission parameters.

## 3. Results and Discussions

In order to explore the PIT effect in the proposed metamaterial, we numerically simulated the transmission curves of the three arrays, including a CRR-only array, an SSRs-only array, and a combination of both, as illustrated in Figure 2a. The terahertz wave is normally incident along the z direction, and electric field polarization is along the y direction. The CRR shows typical electric dipole resonance at 0.54 THz, whereas the SRRs support an inductive-capacitive (LC) resonance at

0.58 THz. It is clear that the CRR-only array has a deeper and broader transmission curve than the SSRs-only array, allowing for a good absorption of the terahertz wave. Thus, resonance from the CRR acts as the bright mode, while resonance from the SSRs is regarded as the dark mode. When both the CRR and the SRRs are combined to form the unit cell, an interesting phenomenon occurs in which a sharp transmission peak emerges at 0.56 THz through near-field coupling between the CRR and SRRs. The narrow transmission window caused by the destructive interference between the bright and dark mode indicates a characteristic feature of the PIT effect.

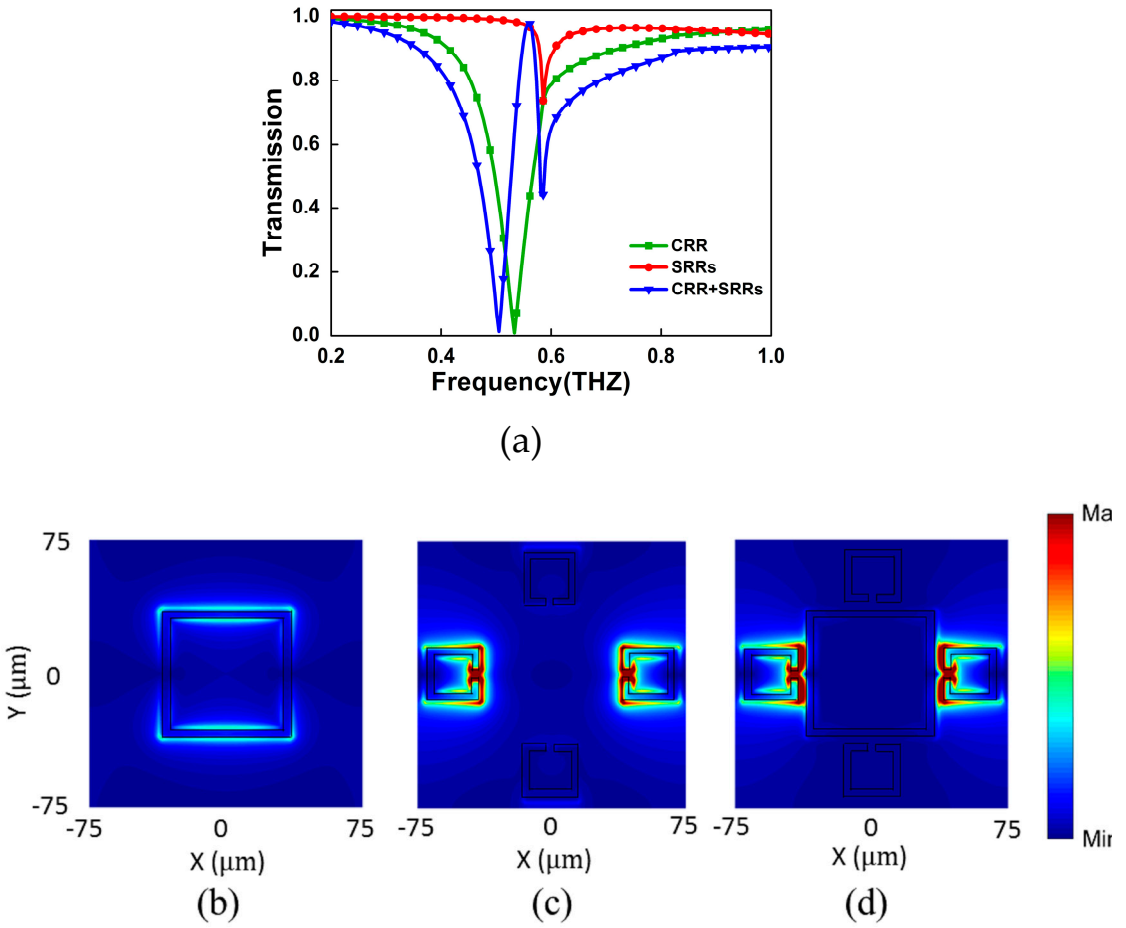


**Figure 2.** (**a**) Simulated transmission spectra for closed square ring resonator (CRR), split ring resonators (SRRs), and CRR+SRRs, respectively. (**b**) Electric field distribution of the CRR at 0.54 THz. (**c**) Electric field distribution of the SRRs at 0.58 THz. (**d**) Electric field distribution of the CRR+SRRs at 0.56 THz.

Furthermore, the induced electric field $E = \sqrt{|E_x|^2 + |E_y|^2 + |E_z|^2}$ distributions of the three arrays at the resonant frequency are exhibited in Figure 2b–d. For the CRR structure, the electric field is mainly concentrated in the two horizontal arms. For the SSRs structure, only two SRRs (aligned with CRR in a horizontal direction) are excited by the incident terahertz wave, and the electric field is mainly focused around the gaps of the two excited SRRs. For the combined CRR and SRRs structure (i.e., the proposed PIT metamaterial), the enhancement of the electric field concentrates around the split gaps of the two previously excited SRRs, while the electric field distribution at the CRR is strongly suppressed because of the electromagnetic coupling effect, which indicate the destructive interference between the bright and dark modes.

Next, single-layer graphene, a two-dimensional flat sheet, was integrated into the unit cell to realize a tunable PIT effect. The transmission spectra corresponding to the unit cell without and with single-layer graphene are plotted in Figure 3a. Without a graphene layer, there is a typical transparent peak with a transmission amplitude of 0.97 at 0.56 THz. In the presence of a graphene layer under the

metal structure, the transmission amplitude of the PIT window is gradually attenuated with the increase of Fermi energy, which provides a way to control the PIT response. For example, the transmission amplitude of the PIT peak changes from 0.69 with $E_F = 0.1$ eV to 0.49 with $E_F = 0.3$ eV without a noteworthy frequency shift. With $E_F = 0.5$ eV, the transparent window is eliminated completely, and only a resonance notch remains at 0.52 THz in the transmission spectra. Finally, the transmission amplitude of the PIT window experiences an on-to-off process by merely shifting Fermi energy without reconstructing the metamaterial structure, which is more desirable for practical applications.

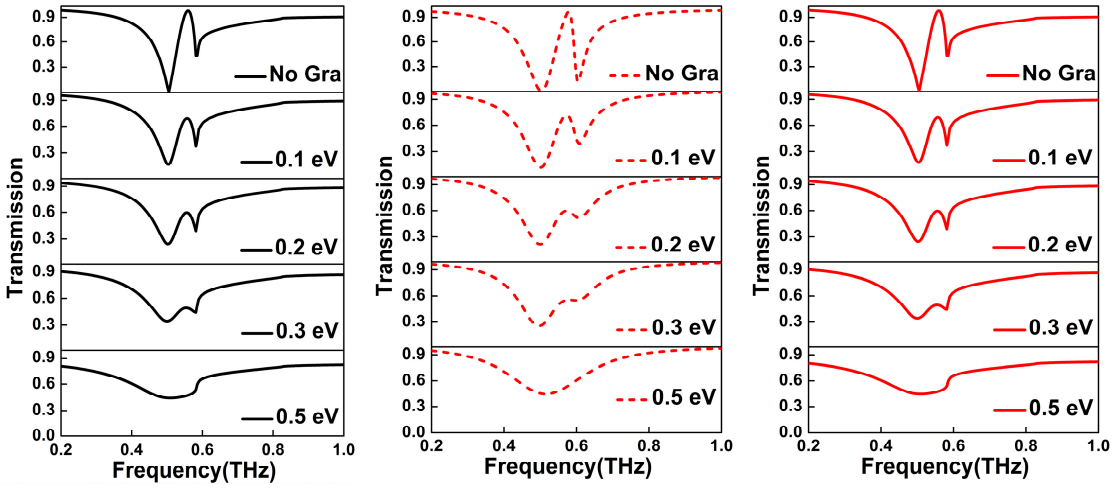


**Figure 3.** Transmission spectra for the proposed PIT structure: (**a**) numerical simulation for incident polarization in the y direction, (**b**) analytical calculation based on the classical coupled two-particle model, and (**c**) numerical simulation for incident polarization in the x direction.

The aforementioned PIT effect modulation behavior is elucidated by the classical coupled two-particle model. In the aluminum-based unit cell, the CRR is considered the bright particle, which is strongly driven by the external electric field $E = E_0 \exp(i\omega t)$, and the SRRs represent the dark particle, which is weakly coupled to the incident terahertz wave. Hence, the interplay between the two particles, radiated by the incident terahertz wave, can be analytically described by the following coupling differential equations [36–38]:

$$\ddot{x}_1(t) + \gamma_1 \dot{x}_1(t) + \omega_1^2 x_1(t) + \kappa^2 x_2(t) = Q_1 E / m_1, \tag{3}$$

$$\ddot{x}_2(t) + \gamma_2 \dot{x}_2(t) + \omega_2^2 x_2(t) + \kappa^2 x_1(t) = Q_2 E / m_2. \tag{4}$$

Here, bright and dark particles are represented by subscripts 1 and 2, respectively. $x_1(x_2)$, $\gamma_1(\gamma_2)$, $\omega_1(\omega_2)$, $Q_1(Q_2)$, and $m_1(m_2)$ are the relatively balanced position displacement, damping rate, resonance angular frequency, effective charge, and effective mass of particle, respectively. The coupling coefficient between the two particles is represented by $\kappa$. It is assumed that the expressions of relatively balanced position displacements are $x_1 = c_1 \exp(i\omega t)$ and $x_2 = c_2 \exp(i\omega t)$. The expressions for $x_1$ and $x_2$ as a function of angular frequency are first derived by solving the coupled equations (3) and (4), as follows:

$$x_1 = \frac{\left(\frac{B}{A}\kappa^2 + \omega^2 - \omega_2^2 + i\omega\gamma_2\right)\frac{Q_1 E}{m_1}}{\kappa^4 - \left(\omega^2 - \omega_1^2 + i\omega\gamma_1\right)\left(\omega^2 - \omega_2^2 + i\omega\gamma_2\right)}, \tag{5}$$

$$x_2 = \frac{\left(\kappa^2 + \frac{B}{A}\left(\omega^2 - \omega_1^2 + i\omega\gamma_1\right)\right)\frac{Q_1 E}{m_1}}{\kappa^4 - \left(\omega^2 - \omega_1^2 + i\omega\gamma_1\right)\left(\omega^2 - \omega_2^2 + i\omega\gamma_2\right)}, \tag{6}$$

where $A = Q_1/Q_2$ and $B = m_1/m_2$ are dimensionless real constants characterizing the relative coupling of the incident electric field with the bright and dark modes. The effective polarization of the system is proportional to the displacement, and the electric susceptibility of the system is related to the effective polarization. Therefore, the displacements of the bright and dark particles can be used to determine the electric susceptibility of the PIT structure as follows:

$$\begin{aligned}\chi &= \chi_r + \chi_i = \frac{P}{\varepsilon_0 E} = \frac{Q_1 x_1 + Q_2 x_2}{\varepsilon_0 E} \\ &= \frac{K}{A^2 B}\left(\frac{A(B+1)\kappa^2 + A^2\left(\omega^2-\omega_2^2\right)+B\left(\omega^2-\omega_1^2\right)}{\kappa^4-\left(\omega^2-\omega_1^2+i\omega\gamma_1\right)\left(\omega^2-\omega_2^2+i\omega\gamma_2\right)} + i\omega\frac{A^2\gamma_2+B\gamma_1}{\kappa^4-\left(\omega^2-\omega_1^2+i\omega\gamma_1\right)\left(\omega^2-\omega_2^2+i\omega\gamma_2\right)}\right)\end{aligned} \tag{7}$$

where $K$ describes the proportionality factor, $\chi_r$ represents the dispersion, and $\chi_i$ shows the absorption within the medium. From this point of view, the transmission can be calculated through the equation $T = 1 - \chi_i$.

The resultant transmission spectra through the metal–graphene PIT metamaterial is calculated based on the classical coupled two-particle model, as shown in Figure 3b. The overall qualitative agreement between the numerical simulation and calculation results is excellent, validating the rationality of the analytical model. In the process of fitting the transmission spectra, we let A = 40, B = 1, considering the weak response of the dark resonator to the incident field in the PIT device. As a result, other corresponding fitting parameters with different Fermi energies are plotted in Figure 4a. Clearly, $\kappa$ and $\gamma_1$ maintain stable values as the Fermi energy changes; however, $\gamma_2$ shows a drastic, almost linear increase from $\gamma_2 = 0.001$ THz for the absence of graphene to $\gamma_2 = 0.38$ THz for the case with $E_F = 0.5$ eV. This indicates that the damping rate $\gamma_2$ of dark SRRs, being an important parameter accounting for the tunable PIT effect, is evidently enhanced with a higher Fermi energy. As the losses in the dark resonator are significantly increased, the LC resonance intensity is evidently decreased. In the PIT structure, the graphene layer with high conductivity, which acts as a channel of charge, shorts the split gaps of the dark SRRs. As the graphene Fermi energy increases, the strong shorting effect of graphene with high conductivity on the capacitive split gaps weakens the surface resonance current of the dark resonator, reducing its LC resonance intensity and effectively suppressing the destructive interference between the bright and dark resonators. With $E_F = 0.5$ eV, the dark mode resonance intensity is too weak to maintain the appearance of PIT resonance. The tunable response is attributed to the dampening of the dark resonator through the conductive graphene layer. Despite the simplicity of the coupled two-particle model, the fitting results predict the function of the graphene layer in the device structure and can be used to further optimize device performance.

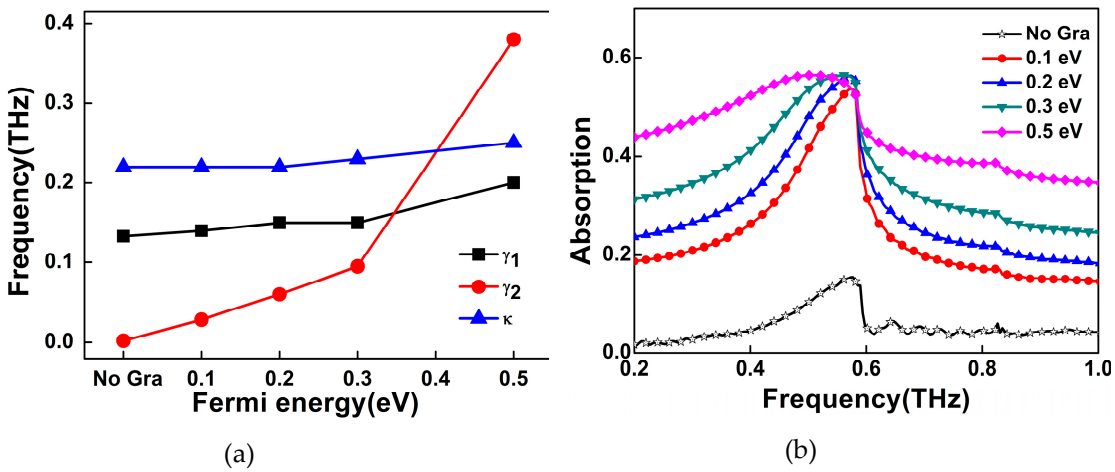


**Figure 4.** (**a**) Extracted fitting parameters of the classical coupled two-particle model for different Fermi energies. (**b**) Calculated absorption spectra with different Fermi energies.

Graphene is coupled with metallic metamaterials to enhance the controllability of the terahertz wave by using a resonance or local electric field enhancement effect. In order to further explore the function of graphene in the PIT active device, the absorption is calculated with the equation $A = 1 - T - R$, where T and R denote the transmission and reflection, respectively. The absorbance spectra, as shown in Figure 4b, are normalized with respect to a bare silicon substrate. In the absence of the graphene layer, there is a very narrow absorption peak at about 0.56 THz, indicating small losses in the coupling system. The absorption enhancement starts once the graphene is introduced. By further increasing the graphene Fermi energy $E_F$, the system losses rise, and the absorption peak grows significantly in strength and linewidth. As a result, the absorption becomes more and more prominent and uncouples the regime between the bright and dark resonators, causing the PIT effect to disappear.

To reveal the tunable mechanism of the proposed metamaterial, the electric field distributions under the incident electric field y-direction polarization are presented in Figure 5 at the PIT resonance frequency. It can be observed that the case without a graphene layer and the case with different Fermi energies for the integrated graphene have similar electric field distributions, despite the intensity difference, which indicate the evolution process of the destructive interference between the bright and dark modes. For the bare aluminum-based PIT structure, the electric field is mainly concentrated in the dark resonator, due to the charge accumulating and electric field focusing caused by the capacitive gaps of the two excited SRRs. The introduction of a metal-like graphene layer provides a charge transmission channel for the capacitive split gaps in the dark mode SRRs. Therefore, the opposite charges on both sides of the capacitive gaps are gradually neutralized and the LC resonance current is weakened, resulting in a suppression of the resonance intensity in the dark resonator. As a result, the weakening resonance intensity in the dark resonator leads to a decoherence effect, thereby weakening the electric field strength in the dark resonator and enhancing it in the bright resonator. With the maximum Fermi energy of 0.5 eV, there is an electric dipole resonance in the bright resonator, similar to the bare bright resonator in Figure 2b, and the electric field is significantly reduced in the dark resonator, indicating that the PIT resonance has been transformed into an isolated electric dipole resonance. In the terahertz regime, graphene, as a conductive film, usually plays a pivotal role in the split gap area, thanks to the obvious shorting effect in the narrow excited capacitive gap. It can be inferred from the above analysis, that the tunability of the PIT metamaterial stems from modulation resonance intensity of the dark mode via varying graphene Fermi energy. The demonstrated concept is generic and applicable for other two-dimensional materials with variable conductive properties.

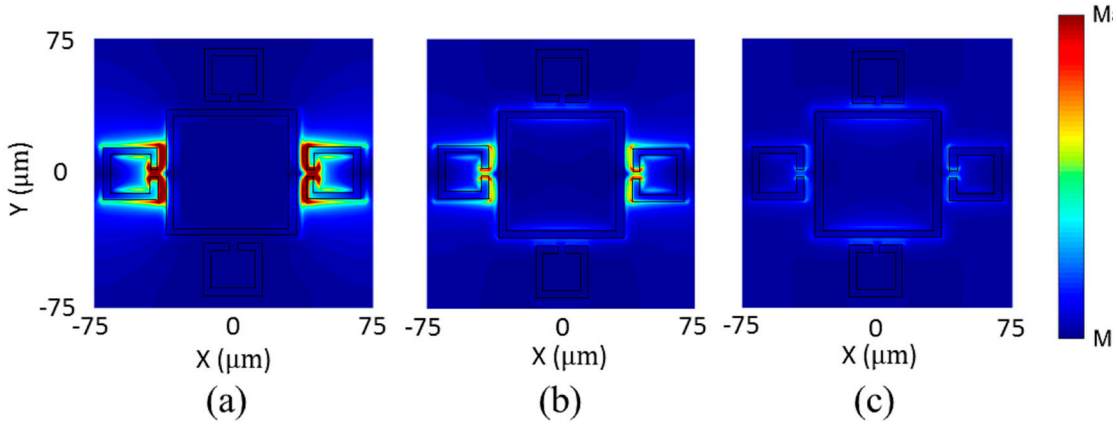


**Figure 5.** Electric field distributions at the resonant frequency for the cases of (**a**) without a graphene layer, (**b**) $E_F = 0.2$ eV, and (**c**) $E_F = 0.5$ eV.

In general, the dynamic response of optical excitation for subwavelength metamaterial elements is sensitive to the polarization of incident light. In order to achieve polarization-independent behavior in PIT metamaterials, the designed structure must have a specific symmetry to maintain the same response

to any polarization of incident light [39]. An important advantage of the proposed structure is the polarization-independent feature. It is evident from Figure 3a,c that the tunable PIT effect is identical for both the x- and y-polarized incident waves. Owing to its fourfold symmetry [40,41], the proposed PIT structure has an identical response for any incident polarization. This behavior can be explained by the fact that an arbitrarily polarized wave can be orthogonally decomposed into x-direction and y-direction polarized waves. The identical resonance curve structures are observed in the transmission spectra for two orthogonal directions, due to the fact that each orthogonal component corresponds to the same structure arrangement. With a change of the polarization angle of incident light, the relative ratio of the two orthogonal components also changes, but the superposition result of electromagnetic response remains unchanged, and the PIT resonance intensity is still constant, which has been verified by the experimental measurements [8]. This polarization-independent PIT device is unaffected by the incident polarization states, effectively expanding its practical application. For example, our device can be conveniently utilized for terahertz sources with an unknown polarization state.

## 4. Conclusions

In summary, the tunable and polarization-independent plasmon-induced transparency in metal-graphene metamaterial was investigated in the terahertz regime. This function can be achieved by merely varying the graphene Fermi energy, which is difficult to obtain in conventional metal-based metamaterial. The designed active device has been fully characterized via the numerical simulation and the classical coupled two-particle model, showing a strength modulation of the PIT resonance and identical response to arbitrary incident polarization. In the work, the shorted function of graphene can be directly extended to other coupling systems including split ring resonators, to further develop its applicability. The presented device architecture provides an interesting platform for further comprehending intriguing light–matter interactions in metamaterials and offers new ideas for the development of terahertz dynamic functional devices such as buffers, modulators, and sensors.

**Author Contributions:** G.W. conceived the idea; X.W. performed the numerical simulations; X.Z. gave the guideline for the study; G.W., X.Z., and G.Z. participated in the discussions and writing the article.

**Funding:** This research was funded by the National Natural Science Foundation of China (Nos.61377036 and 60971015) and The Science and Technology Coordination Innovation Project of Shaanxi province (No. S2018-ZC-PT-0024).

**Acknowledgments:** We express our deep gratitude to Lei Zhang (Xi'an Jiaotong University) for a helpful discussion and technical support with the numerical simulation.

**Conflicts of Interest:** The authors declare no conflict of interest.

## References

1. Zhang, Y.; Yang, Q.; Deng, B.; Qin, Y.; Wang, H. Experimental research on interferometric inverse synthetic aperture radar imaging with multi-channel terahertz radar system. *Sensors* **2019**, *19*, 2330. [CrossRef]
2. Niessen, K.A.; Xu, M.; George, D.K.; Chen, M.C.; Ferré-D'Amaré, A.R.; Snell, E.H.; Cody, V.; Pace, J.; Schmidt, M.; Markelz, A.G. Protein and RNA dynamical fingerprinting. *Nat. Commun.* **2019**, *10*, 1026. [CrossRef] [PubMed]
3. García-Muñoz, E.; Abdalmalak, K.A.; Santamaría, G.; Rivera-Lavado, A.; Segovia-Vargas, D.; Castillo-Araníbar, P.; Van Dijk, F.; Nagatsuma, T.; Brown, E.R.; Guzman, R.C.; et al. Photonic-based integrated sources and antenna arrays for broadband wireless links in terahertz communications. *Semicond. Sci. Technol.* **2019**, *34*, 054001. [CrossRef]
4. Zheludev, N.I. The road ahead for metamaterials. *Science* **2010**, *328*, 582–583. [CrossRef] [PubMed]
5. Chen, H.T.; Padilla, W.J.; Zide, J.M.; Gossard, A.C.; Taylor, A.J.; Averitt, R.D. Active terahertz metamaterial devices. *Nature* **2006**, *444*, 597–600. [CrossRef]
6. Chen, H.-T.; Padilla, W.J.; Cich, M.J.; Azad, A.K.; Averitt, R.D.; Taylor, A.J. A metamaterial solid-state terahertz phase modulator. *Nat. Photonics* **2009**, *3*, 148–151. [CrossRef]

7. Liu, M.; Yang, Q.; Xu, Q.; Chen, X.; Tian, Z.; Gu, J.; Ouyang, C.; Zhang, X.; Han, J.; Zhang, W. Tailoring mode interference in plasmon-induced transparency metamaterials. *J. Phys. D: Appl. Phys.* **2018**, *51*, 174005. [CrossRef]
8. Liu, M.; Tian, Z.; Zhang, X.; Gu, J.; Ouyang, C.; Han, J.; Zhang, W. Tailoring the plasmon-induced transparency resonances in terahertz metamaterials. *Opt. Express* **2017**, *25*, 19844–19855. [CrossRef]
9. Cong, L.; Xu, N.; Chowdhury, D.R.; Manjappa, M.; Rockstuhl, C.; Zhang, W.; Singh, R. Nonradiative and radiative resonances in coupled metamolecules. *Adv. Opt. Mater.* **2016**, *4*, 252–258. [CrossRef]
10. Chen, H.; Zhang, H.; Guo, X.; Liu, S.; Zhang, Y. Tunable plasmon-induced transparency in H-shaped Dirac semimetal metamaterial. *Appl. Opt.* **2018**, *57*, 752–756. [CrossRef]
11. Zhang, Z.; Yang, J.; He, X.; Han, Y.; Zhang, J.; Huang, J.; Chen, D.; Xu, S. Plasmon-induced transparency based on aperture-coupled cascade resonators without gap. *Superlattices Microstruct.* **2018**, *123*, 138–143. [CrossRef]
12. Hokmabadi, M.P.; Philip, E.; Rivera, E.; Kung, P.; Kim, S.M. Plasmon-induced transparency by hybridizing concentric-twisted double split ring resonators. *Sci. Rep.* **2015**, *5*, 15735. [CrossRef] [PubMed]
13. Liu, C.; Liu, P.; Bian, L.; Zhou, Q.; Li, G.; Liu, H. Dynamically tunable electromagnetically induced transparency analogy in terahertz metamaterial. *Opt. Commun.* **2018**, *410*, 17–24. [CrossRef]
14. Wei, B.; Liu, H.; Ren, G.; Yang, Y.; Ye, S.; Pei, L.; Jian, S. Graphene based silicon–air grating structure to realize electromagnetically-induced-transparency and slow light effect. *Phys. Lett. A* **2017**, *381*, 160–165. [CrossRef]
15. Zhang, S.; Genov, D.A.; Wang, Y.; Liu, M.; Zhang, X. Plasmon-induced transparency in metamaterials. *Phys. Rev. Lett.* **2008**, *101*, 047401. [CrossRef]
16. Sun, C.; Si, J.; Dong, Z.; Deng, X. Tunable multispectral plasmon induced transparency based on graphene metamaterials. *Opt. Express* **2016**, *24*, 11466–11474. [CrossRef]
17. Tassin, P.; Koschny, T.; Soukoulis, C.M. Applied physics. Graphene for terahertz applications. *Science* **2013**, *341*, 620–621. [CrossRef]
18. Neto, A.H.C.; Guinea, F.; Peres, N.M.R.; Novoselov, K.S.; Geim, A.K. The electronic properties of graphene. *Rev. Mod. Phys.* **2009**, *81*, 109–162. [CrossRef]
19. Li, X.; Tao, L.; Chen, Z.; Fang, H.; Li, X.; Wang, X.; Xu, J.-B.; Zhu, H. Graphene and related two-dimensional materials: Structure-property relationships for electronics and optoelectronics. *Appl. Phys. Rev.* **2017**, *4*, 021306. [CrossRef]
20. Chen, D.-C.; Li, H.-J.; Xia, S.-X.; Qin, M.; Zhai, X.; Wang, L.-L. Dynamically tunable electromagnetically-induced-transparency–like resonances in graphene nanoring and nanodisk hybrid metamaterials. *Europhys. Lett.* **2017**, *119*, 47002. [CrossRef]
21. Qian, Z.; Yang, D.; Wang, W. Terahertz modulation based on surface plasmon resonance by self-gated graphene. *Opt. Commun.* **2018**, *414*, 52–58. [CrossRef]
22. He, X.; Yang, X.; Lu, G.; Yang, W.; Wu, F.; Yu, Z.; Jiang, J. Implementation of selective controlling electromagnetically induced transparency in terahertz graphene metamaterial. *Carbon* **2017**, *123*, 668–675. [CrossRef]
23. Low, T.; Avouris, P. Graphene Plasmonics for Terahertz to Mid-Infrared Applications. *ACS Nano* **2014**, *8*, 1086–1101. [CrossRef]
24. Degl'Innocenti, R.; Jessop, D.S.; Shah, Y.D.; Sibik, J.; Zeitler, J.A.; Kidambi, P.R.; Hofmann, S.; Beere, H.E.; Ritchie, D.A.; Zeitler, A. Low-bias terahertz amplitude modulator based on split-ring resonators and graphene. *ACS Nano* **2014**, *8*, 2548–2554. [CrossRef]
25. Wang, G.; Zhang, X.; Zhang, L.; Wei, X. Dynamically tunable plasmon-induced transparency based on radiative–radiative-coupling in a terahertz metal–graphene metamaterial. *Crystals* **2019**, *9*, 146. [CrossRef]
26. Liu, T.; Wang, H.; Liu, Y.; Xiao, L.; Yi, Z.; Zhou, C.; Xiao, S. Active manipulation of electromagnetically induced transparency in a terahertz hybrid metamaterial. *Opt. Commun.* **2018**, *426*, 629–634. [CrossRef]
27. Kakenov, N.; Ergoktas, M.S.; Balci, O.; Kocabas, C. Graphene based terahertz phase modulators. *2D Mater.* **2018**, *5*, 035018. [CrossRef]
28. Tasolamprou, A.C.; Koulouklidis, A.D.; Daskalaki, C.; Mavidis, C.P.; Kenanakis, G.; Deligeorgis, G.; Viskadourakis, Z.; Kuzhir, P.; Tzortzakis, S.; Kafesaki, M.; et al. Experimental demonstration of ultrafast THz modulation in a graphene-based thin film absorber through negative photoinduced conductivity. *ACS Photonics* **2019**, *6*, 720–727. [CrossRef]

29. Dong, Z.; Sun, C.; Si, J.; Deng, X. Tunable polarization-independent plasmonically induced transparency based on metal-graphene metasurface. *Opt. Express* **2017**, *25*, 12251–12259. [CrossRef]
30. Sun, C.; Dong, Z.; Si, J.; Deng, X. Independently tunable dual-band plasmonically induced transparency based on hybrid metal-graphene metamaterials at mid-infrared frequencies. *Opt. Express* **2017**, *25*, 1242–1250. [CrossRef]
31. Huang, H.; Xia, H.; Guo, Z.; Li, H.; Xie, D. Polarization-insensitive and tunable plasmon induced transparency in a graphene-based terahertz metamaterial. *Opt. Commun.* **2018**, *424*, 163–169. [CrossRef]
32. Ordal, M.A.; Bell, R.J.; Alexander, R.W.; Long, L.L.; Querry, M.R. Optical properties of fourteen metals in the infrared and far infrared: Al, co, cu, au, fe, pb, mo, ni, pd, pt, ag, ti, v, and w. *Appl. Opt.* **1985**, *24*, 4493–4499. [CrossRef]
33. Ishikawa, A.; Tanaka, T. Plasmon hybridization in graphene metamaterials. *Appl. Phys. Lett.* **2013**, *102*, 253110. [CrossRef]
34. Jnawali, G.; Rao, Y.; Yan, H.; Heinz, T.F. Observation of a transient decrease in terahertz conductivity of single-layer graphene induced by ultrafast optical excitation. *Nano Lett.* **2013**, *13*, 524–530. [CrossRef] [PubMed]
35. Zhang, Y.; Tan, Y.W.; Stormer, H.L.; Kim, P. Experimental observation of the quantum Hall effect and Berry's phase in graphene. *Nature* **2005**, *438*, 201–204. [CrossRef] [PubMed]
36. Manjappa, M.; Chiam, S.-Y.; Cong, L.; Bettiol, A.A.; Zhang, W.; Singh, R. Tailoring the slow light behavior in terahertz metasurfaces. *Appl. Phys. Lett.* **2015**, *106*, 181101. [CrossRef]
37. Meng, F.-Y.; Wu, Q.; Erni, D.; Wu, K.; Lee, J.-C. Polarization-independent metamaterial analog of electromagnetically induced transparency for a refractive-index-based sensor. *IEEE Trans. Microw. Theory Tech.* **2012**, *60*, 3013–3022. [CrossRef]
38. Zhang, X.; Li, Q.; Cao, W.; Gu, J.; Singh, R.; Tian, Z.; Han, J.; Zhang, W. Polarization-independent plasmon-induced transparency in a fourfold symmetric terahertz metamaterial. *IEEE J. Sel. Top. Quantum Electron.* **2013**, *19*, 8400707. [CrossRef]
39. Papasimakis, N.; Fu, Y.H.; Fedotov, V.A.; Prosvirnin, S.L.; Tsai, D.P.; Zheludev, N. Metamaterial with polarization and direction insensitive resonant transmission response mimicking electromagnetically induced transparency. *Appl. Phys. Lett.* **2009**, *94*, 211902. [CrossRef]
40. Hu, S.; Liu, D.; Lin, H.; Chen, J.; Yi, Y.; Yang, H. Analogue of ultra-broadband and polarization-independent electromagnetically induced transparency using planar metamaterial. *J. Appl. Phys.* **2017**, *121*, 123103. [CrossRef]
41. Duan, X.; Chen, S.; Yang, H.; Cheng, H.; Li, J.; Liu, W.; Gu, C.; Tian, J. Polarization-insensitive and wide-angle plasmonically induced transparency by planar metamaterials. *Appl. Phys. Lett.* **2012**, *101*, 143105. [CrossRef]